Sys Rev Pharm 2020;11(11):453-458
A multifaceted review journal in the field of pharmacy

Hydrothermal Synthesis Of Γ-Mno_2 Nanostructures With Different Morphologies Using Different Mn^{+2} Precursors

Zahraa Hasan Raheem[1], Abdulkareem Mohammed Ali Al-Sammarraie*[2]

1,2 Department of chemistry, College of science, University of Baghdad., Baghdad, Iraq
Corresponding Author: muraee@gmail.com

ABSTRACT

As best of our knowledge this is the first time to obtain MnO2 nanostructures with different morphologies without any use of surfactants, templates or acidic conditions. Three different crystal shapes(cross, sheet, and star) of nanostructure pure phase of γ -MnO2 have been successfully synthesized by hydrothermal method at same conditions of temperature (160ºC) , time of reaction(12 h) and the same mole ratio between the oxidizing agent NaClO3 and the Mn+2 precursor (2:1), the only difference was using different Mn+2 precursor (MnSO4.H2O, MnCl2.4H2O and Mn(OAc)2 .4H2O) separately, the prepared samples had been characterized by using field emission scanning electron microscopy (FE-SEM), x-ray diffraction analysis(XRD) FT-IR spectroscopy, Raman spectroscopy, and Brunauer-Emmett-Teller (BET) surface area analysis. The sample with the highest value of surface area was the sample prepared from MnSO4.H2O (9.163 m2/g) which had a star likeshape. Also the values of De Wolff and micro-twinning defects have been calculated.

Keywords: gamma MnO2, microtwinning, BET, hydrothermal, Mn-percursors

Correspondence:
Abdulkareem Mohammed Ali Al-Sammarraie
1,2 Department of chemistry, College of science, University of Baghdad., Baghdad, Iraq

*Corresponding author: Abdulkareem Mohammed Ali Al-Sammarraie email-address: muraee@gmail.com

INTRODUCTION

In the resent years manganese dioxide has attracted great interest in both scientific and industrial fields due to its special physical and chemical properties, these properties made it an important material in many applications, such as rechargeable batteries and supercapacitors [1-5] , biosensors[6,7] , and catalysis[8-10]. This verity in MnO_2 functionality is because it exists in different crystallographic polymorphs, such as α, β, γ, δ, λ and ε. These polymorphs differ in the way that the octahedral MnO_6 units are connected together by sharing edges or corners of each other which leads to different tunnel structures and sizes or may form a layered structure in the case of δ-MnO_2 [11-14]. γ -MnO_2 is extensively used as a cathode material in alkaline batteries as well as in lithium batteries due to its remarkable structure, high electrochemical activity, low cost, natural abundance and environmental safety. γ -MnO_2 has a complicated structure as shown in Figure (1) which can be considered as a random intergrowth of various amounts of pyrolusite phase (1x1) within a ramsdelite phase (1x2) as the model first described by De Wolff [15] .

Over the last years MnO_2 nanostructures with different morphologies and crystallographic forms have been prepared widely and successfully by using different preparation methods, such as co-precipitation[16,17], sol-gel[18,19], electrodeposition[20,21] and hydrothermal method. Among these different methods, hydrothermal is the most widely used to prepare highly pure nanostructures with easy ability to control phase and morphology [22, 23, 24]. From experiments accomplished by other researches, MnO_2 with different morphologies had been prepared but either with the addition of surfactant [25] or by adding concentrated acid [26, 27, 28]. This work is aimed to obtain MnO_2 nanostructures with different morphologies without any use of surfactants, templates or acidic conditions.

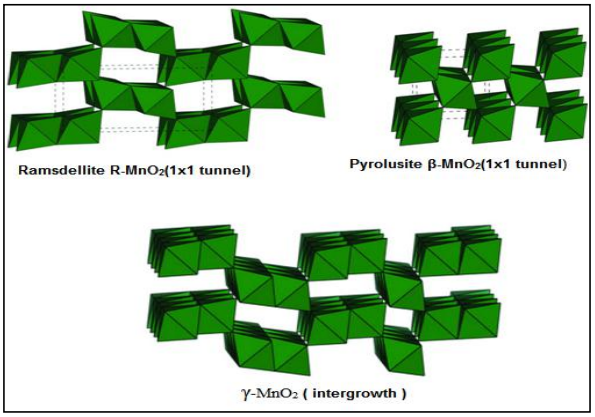

Figure 1: γ-MnO_2 structure .

MATERIALS AND METHODS

All chemicals were used without further purification

Synthesis procedure:

Nanostructured γ -MnO_2 were synthesized by the reaction between $NaClO_3$ (2 m.mole) as an oxidizing agent and (1m.mole) of Mn^{+2} sources from three different salts ($MnSO_4.H_2O$, $MnCl_2.4H_2O$ and $Mn(OAc)_2.4H_2O$) each salt separately. After taking weight of the starting materials they were dissolved in distilled water and magnetically stirred till the solution became clear, then transferred into 100 ml Teflon liner and hydrothermally treated at 160º C for 12 hours, after that it has been left to cool down naturally. Then the dark brown precipitate of γ -MnO_2 was collected and washed several times with distilled water and ethanol and then it was dried at 60ºC for 12 hours.

Characterization:

To determine the phase of the prepared γ -MnO_2 samples X-ray powder diffraction (XRD) patterns of all prepared material have been measured on a Shimadzu (XRD 6000) x-ray diffractometer with Cu Kα radiation (λ=1.54056A°). The size and morphology have been examined with field emission scanning electron microscopy (FESEM Hitachi s-4160).FTIR spectroscopic analysis was done using

Shimadzu (FT-IR 8400S). Surface area of the prepared samples was done with N_2 adsorption at 77.35K.

RESULTS AND DISCUSSION

The reaction between the oxidizing agent $NaClO_3$ and the Mn^{+2} precursors in the three experiments had been done in the same conditions of temperature (160º C), reaction time (12 h) and with the same mole ratio of the starting materials (2:1). From the FE-SEM images shown in Figure (2) the morphologies of the prepared samples are completely different, when $MnSO_4.H_2O$ was used the morphology was six branched crystal or a star like shape with dimensions of (diameter ~140 nm near the center of the star shape and around 55-70nm near the tips, and with variable lengths about 1.5-8 µm), when $MnCl_2.4H_2O$ was used the morphology was very thin hexagonal sheets with thickness about (9-13 nm) and length about 500nm, while when $Mn(OAc)_2.4H_2O$ was used four branched or a cross like shapes were obtained with dimensions of (diameter about 110nm near the center and it becomes thinner near the tips about 50 nm , and the length between 3 to 5 µm).

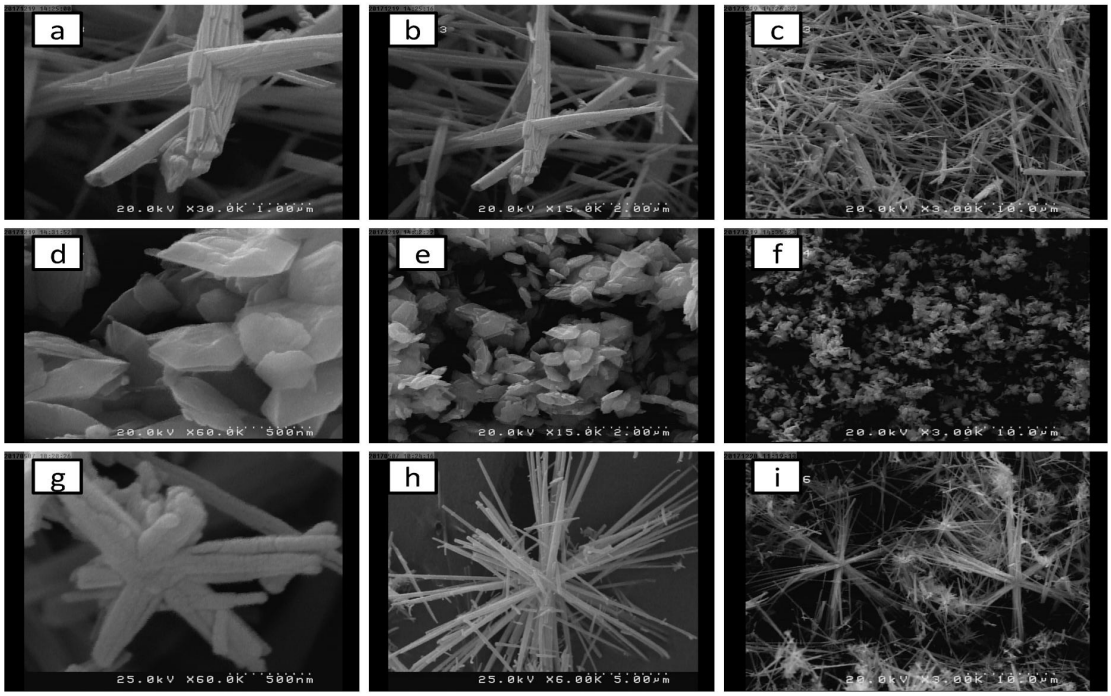

Fig(2): FE-SEM images of (a,b,c) γ -MnO_2 using $Mn(OAc)_2.4H_2O$ as a precursor,(c,d,f) γ -MnO2 using $MnCl_2.4H_2O$ as a precursor, and (g,h,i) γ -MnO_2 using $MnSO_4.H_2O$ as a precursor in different magnifications.

The XRD pattern of all samples as it is illustrated in Figure (3) showed peaks which indicates that all prepared MnO_2 samples are pure gamma phase with no peaks for any other phase, which is an evidence that the mole ratio between the oxidizing agent (ClO_3^{-1}) and Mn^{+2} precursor at 160 ºC is the driving force of gamma MnO_2 formation and the negative part of the Mn^{+2} salts may be the reason of the different morphologies, the peaks are sharp and clear which means that all samples have good crystallite nature.

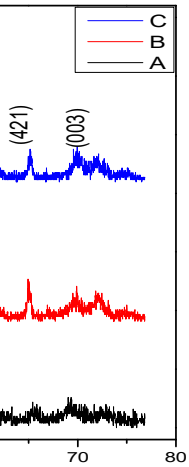

Fig(3) shows the XRD patterns of :(A) γ -MnO_2 prepared from $MnCl_2.4H_2O$ as a precursor,(B) γ -MnO_2 from $MnSO_4.H_2O$ as a precursor, and (C) γ -MnO_2 $Mn(OAc)_2.4H_2O$ as a precursor

The x- ray diffraction analysis can reveal the phase of the crystal structures, it also gives an indication of the purity and the crystalline nature of the materials. All the diffraction peaks can be clearly indexed to pure phase of orthorhombic γ -MnO_2 and the peaks are with a good agreement with the standard reported data(JCPDS card No. 14-644, with lattice parameters a= 6.36Aº , b=10.15 Aº and c=4.09 Aº), and the diffraction peaks of the three samples are slightly different that is due to the difference in the values of the fraction of the pyrolusite within γ -MnO_2 which is expressed in literatures by (P_r) or De Wolff disorder, also there is another type of disorders which is microtwinning defect from the twinning of(002) and(061) planes , these values can be evaluated from the XRD patterns of γ -MnO_2 using the models described by Chabre and Pannetier [29] as shown in the following equations:

$Tw = 100 - 25.20\ (\Delta 2\theta)$ (1)

where ($\Delta 2\theta$ is the splitting between(002) and(061)

$Pr = 0.602.\delta\ (DW) - 0.198\ \delta^2(DW) + 0.026\ \delta^3(DW)$ (2)

$\delta\ (DW) = 2\theta\ (110) - \delta(Tw) - 21.808$ (in degrees) (3)

$\delta(Tw) = - 0.0054\ Tw - 8.9x10^{-5}\ Tw^2$ (in degrees) (4)

Where δ (DW) is the shift of (110) due to microtwinning, and δ(Tw) is the theoretical shift of line (110) . And the values of Pr and Tw are listed in table (1):

Table (1) : calculated values of Pr and Tw for the three prepared γ -MnO_2.

sample	Precursor	Pr	Tw(%)
A	$MnCl_2.4H_2O$	0.428	24%
B	$MnSO_4.H_2O$	0.471	20%
C	$Mn(OAc)_2.4H_2O$	0.612	14%

When the XRD patterns of γ -MnO_2 are compared with the typical XRD peaks of the ramsdellite, some differences can be observed of the (110) reflection of 2θ (22º) which can be shifted to higher angles if there is higher amounts of pyrolusite phase intergrowth , the values of these angles for the prepared samples for γ -MnO_2 from $MnCl_2.4H_2O$ precursor 2θ for (110) reflection was 22.62º which was lower than the other samples which both had values of 22.86º. Also the larger the splitting between reflections (110) and (130) , the smaller the amount of P_r [30]. It is important to evaluate the amount of P_r because it can have great influence on the reactivity of γ -MnO_2. γ -MnO_2 samples with larger values of P_r have more planner oxygen atoms in there structures which are incompletely coordinated giving them more ability to react with protons and drawing the electron density from the surface oxygen atoms and this will decrease the ability of γ -MnO_2 to adsorb divalent ions (such as Zn^{+2}, Cd^{+2}, Pb^{+2} and other ions), hence changing the surface properties of γ -MnO_2 structures[31,32] . From table (1) sample A showed the lowest value of Pr and highest value of microtwinning. The Brunauer-Emmett-Teller (BET) surface area analysis was done to determine the surface area of the samples by first degassing the samples at (200 ºC) for two hours , and the analysis showed that the samples had surface area of (4.047 m^2/g ,8.97 m^2/g ,and 9.163 m^2/g) for sample prepared using $MnCl_2.4H_2O$, $Mn(OAc)_2.4H_2O$, $MnSO_4.H_2O$ respectively .The FT-IR spectra of the three samples in Fig (5) shows several absorption bands, the absorption around 3400 cm^{-1} is usually attributed to the (-OH) stretching vibration mode [33]. The absorption at about 1620 cm^{-1} is due to the(-OH) bending vibration mode which are combined with Mn atoms, this band is a characteristic absorption band of the water of crystallization in the γ -MnO_2 phase, also the γ -MnO_2 shows bands around (515-600) cm^{-1} which is attributed to the Mn-O vibrations in the [MnO_6] octahedral structures[34,35].

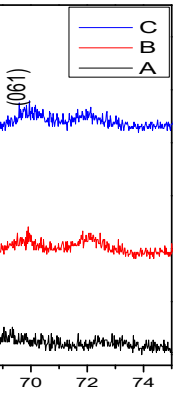

Figure (4): XRD pattern of the three samples showing the splitting between (221)/(240) and (002)/(061) planes.

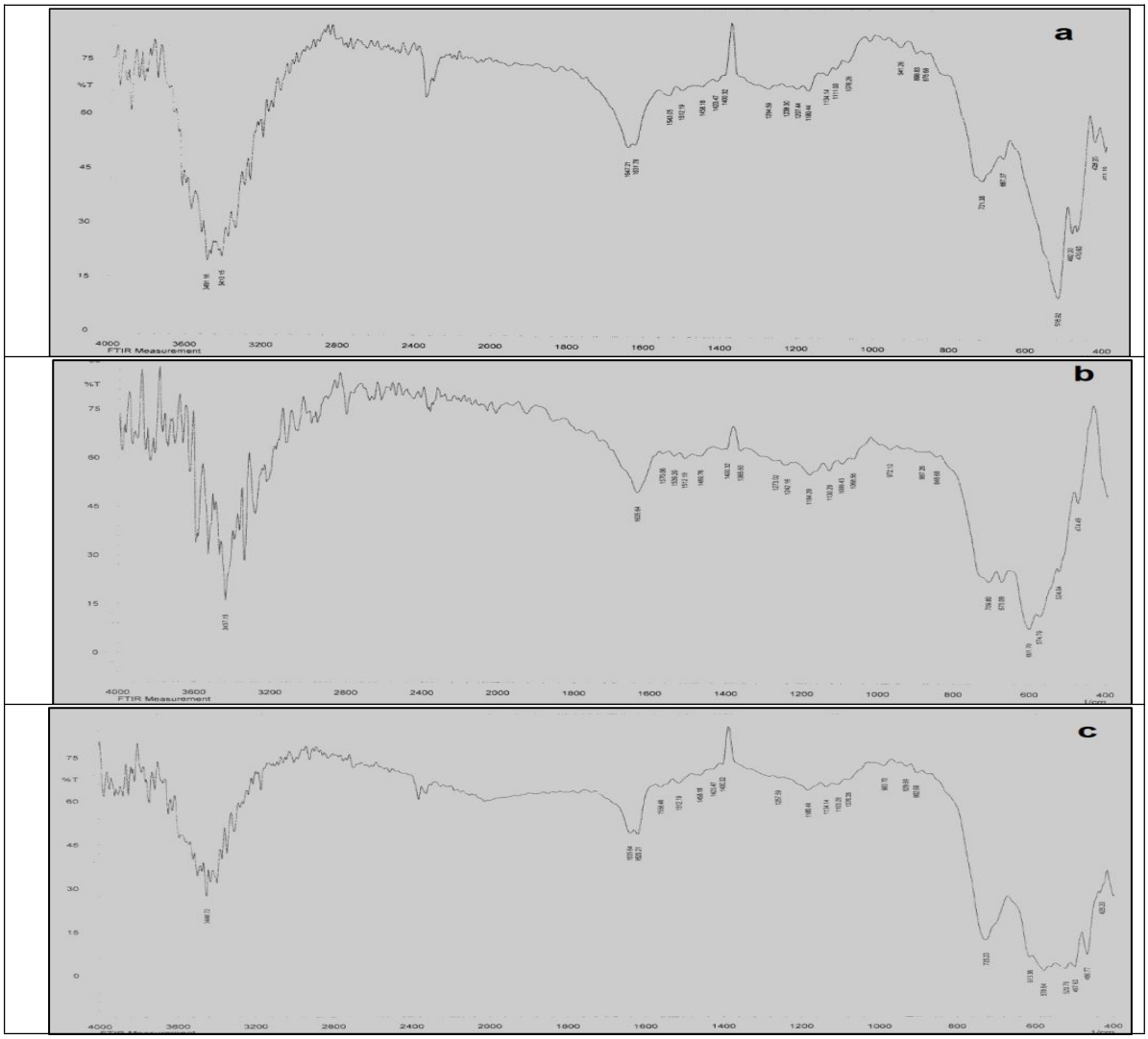

Fig (5) : FT-IR spectra of (a) γ -MnO_2 using $Mn(OAc)_2.4H_2O$ as a precursor (b) γ -MnO2 using $MnCl_2.4H_2O$ as a precursor ,and (c) γ -MnO_2 using $MnSO_4.H_2O$ as a precursor.

Raman scattering spectroscopy is a useful and an important technique to determine the different phases of manganese dioxide as well as the structural defects in γ -MnO_2 phase. Fig (6) shows Raman scattering spectra for the three prepared samples, and it clearly shows that the three samples have the same pattern ,the peaks in the region between (500-700cm^{-1}) are characteristic for γ -MnO_2 [36], the peaks at 576 and 658cm^{-1} are attributed to stretching mode of Mn-O bond in the [MnO_6] octahedral units [22] . If the peak at 658cm^{-1} is more intense that is an indication for more Pr (or more pyrolusite intergrowth) in the samples [37], from Fig. (6) sample (C) shows more intense peaks at this wave number. Which is consistent with the XRD results.

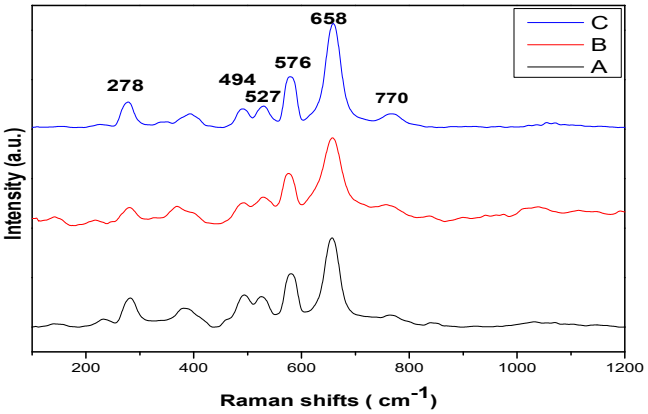

Fig (6): Raman scattering spectra of γ -MnO_2 (A) prepared from $MnCl_2.4H_2O$ (B) prepared from $MnSO_4.H_2O$ and (C) prepared from $Mn(OAc)_2.4H_2O$.

CONCLUSIONS

Three different crystal shapes of γ -MnO_2 nanostructures have been hydrothermally prepared using three different Mn^{+2} precursors but with the same conditions of temperature, time of reaction and mole ratio, the different morphologies obtained in this work is probably due to the negative part of the three Mn^{+2} salts ($Mn(OAc)_2.4H_2O$, $MnCl_2.4H_2O$,and $MnSO_4.H_2O$) used to prepare γ -MnO_2. The sample with the highest value of surface area was sample B prepared from $MnSO_4.H_2O$ (9.163 m^2/g) which had a star like. The values of De Wolff pyrolusite and microtwinning defects was (Pr =0.428 ,Tw=24% for sample A), (Pr =0.471 ,Tw=20% for sample B) and(Pr =0. 0.612 ,Tw=14% for sample C) sample A showed the highest value for micro-twinning and lowest value of pyrolusite.

REFERENCES

1. Cheng, F., Zhao, J., Song, W., Li, C., Ma, H., Chen, J., & Shen, P. (2006). Facile controlled synthesis of MnO2 nanostructures of novel shapes and their application in batteries. *Inorganic chemistry*, *45*(5), 2038-2044.
2. Li, B., Rong, G., Xie, Y., Huang, L., & Feng, C. (2006). Low-temperature synthesis of α-MnO2 hollow urchins and their application in rechargeable Li^+ batteries. *Inorganic chemistry*, *45*(16), 6404-6410.
3. Chen, S., Zhu, J., Han, Q., Zheng, Z., Yang, Y., & Wang, X. (2009). Shape-controlled synthesis of one-dimensional MnO2 via a facile quick-precipitation procedure and its electrochemical properties. *Crystal Growth & Design*, *9*(10), 4356-4361.
4. Jia, Z., Wang, J., Wang, Y., Li, B., Wang, B., Qi, T., & Wang, X. (2016). Interfacial Synthesis of δ-MnO2 Nano-sheets with a Large Surface Area and Their Application in Electrochemical Capacitors. *Journal of Materials Science & Technology*, *32*(2), 147-152.
5. Zhao, J., Tao, Z., Liang, J., & Chen, J. (2008). Facile synthesis of nanoporous γ-MnO_2 structures and their application in rechargeable Li-ion batteries. *Crystal Growth and Design*, *8*(8), 2799-2805.
6. Bai, Y. H., Du, Y., Xu, J. J., & Chen, H. Y.(2007). Choline biosensors based on a bi-electrocatalytic property of MnO 2 nanoparticles modified electrodes to H_2O_2 . *Electrochemistry Communications*, *9*(10), 2611-2616.
7. Liu, Y., Zhang, X., He, D., Ma, F., Fu, Q., & Hu, Y. (2016). An amperometric glucose biosensor based on a MnO_2/graphene composite modified electrode. *RSC Advances*, *6*(22), 18654-18661.
8. Yuan, H., Deng, L., Qi, Y., Kobayashi, N., & Hasatani, M. (2015). Morphology-dependent performance of nanostructured MnO2 as an oxygen reduction catalyst in microbial fuel cells.
9. Ramesh, K., Chen, L., Chen, F., Liu, Y., Wang, Z., & Han, Y. F. (2008). Re-investigating the CO oxidation mechanism over unsupported MnO, Mn_2O_3 and MnO_2 catalysts. *Catalysis Today*, *131*(1), 477-482.
10. Zhang, J., Li, Y., Wang, L., Zhang, C., & He, H. (2015). Catalytic oxidation of formaldehyde over manganese oxides with different crystal structures. *Catalysis Science & Technology*, *5*(4), 2305-2313.
11. Post, J. E. (1999). Manganese oxide minerals: Crystal structures and economic and environmental significance. *Proceedings of the National Academy of Sciences*, *96*(7), 3447-3454.
12. Thackeray, M. M. (1997). Manganese oxides for lithium batteries. *Progress in Solid State Chemistry*, *25*(1-2), 1-71.
13. Feng, Q., Kanoh, H., & Ooi, K. (1999). Manganese oxide porous crystals. *Journal of Materials Chemistry*, *9*(2), 319-333.
14. Wei, W., Cui, X., Chen, W., & Ivey, D. G. (2011). Manganese oxide-based materials as electrochemical supercapacitor electrodes. *Chemical society reviews*, *40*(3), 1697-1721.
15. De Wolff, P. M. (1959). Interpretation of some γ-MnO2 diffraction patterns. *Acta Crystallographica*, *12*(4), 341-345.
16. Kanha, P., & Saengkwamsawang, P. (2017). Effect of stirring time on morphology and crystalline features of MnO2 nanoparticles synthesized by co-precipitation method. *Inorganic and Nano-Metal Chemistry*, *47*(8), 1129-1133.
17. Cherian, E., Rajan, A., & Baskar, G. (2016). Synthesis of manganese dioxide nanoparticles using co-precipitation method and its antimicrobial activity.
18. Ching, S., Petrovay, D. J., Jorgensen, M. L., & Suib, S. L. (1997). Sol− gel synthesis of layered birnessite-type manganese oxides. *Inorganic Chemistry*, *36*(5), 883-890.
19. Wang, X., Yuan, A., & Wang, Y. (2007). Supercapacitive behaviors and their temperature dependence of sol–gel synthesized nanostructured manganese dioxide in lithium hydroxide electrolyte. *Journal of Power Sources*, *172*(2), 1007-1011.
20. Chou, S., Cheng, F., & Chen, J. (2006). Electrodeposition synthesis and electrochemical properties of nanostructured γ-MnO_2 films. *Journal of Power Sources*, *162*(1), 727-734.
21. Dang, T. D., Le, T. T. H., Hoang, T. B. T., & Mai, T. T. (2015). Synthesis of nanostructured manganese oxides based materials and application for supercapacitor . *Advances in Natural Sciences: Nanoscience and Nanotechnology*, *6*(2), 025011.
22. Dong, Y., Li, K., Jiang, P., Wang, G., Miao, H., Zhang, J., & Zhang, C. (2014). Simple hydrothermal preparation of α-, β-, and γ-MnO_2 and phase sensitivity in catalytic ozonation. *RSC Advances*, *4*(74), 39167-39173.
23. Cheng, F., Zhao, J., Song, W., Li, C., Ma, H., Chen, J., & Shen, P. (2006). Facile controlled synthesis of MnO_2 nanostructures of novel shapes and their application in batteries. *Inorganic chemistry*, *45*(5), 2038-2044.
24. Luo, J., Zhu, H. T., Fan, H. M., Liang, J. K., Shi, H. L., Rao, G. H., ... & Shen, Z. X. (2008). Synthesis of single-crystal tetragonal α-MnO_2 nanotubes. *The Journal of Physical Chemistry C*, *112*(33), 12594-12598.
25. Song, X. C., Zhao, Y., & Zheng, Y. F. (2007). Synthesis of MnO_2 nanostructures with sea urchin shapes by a sodium dodecyl sulfate-assisted hydrothermal process. *Crystal growth & design*, *7*(1), 159-162.
26. Wu, J., Huang, H., Yu, L., & Hu, J. (2013). Controllable hydrothermal synthesis of MnO_2 nanostructures. *Advances in Materials Physics and Chemistry*, *3*(03), 201.
27. Feng, J. J., Zhang, P. P., Wang, A. J., Zhang, Y., Dong, W. J., & Chen, J. R. (2011). One-pot hydrothermal synthesis of uniform β-MnO_2 nanorods for nitrite sensing. *Journal of colloid and interface science*, *359*(1), 1-8.

28. Liu, Y., Zhang, M., Zhang, J., & Qian, Y. (2006). A simple method of fabricating large-area α-MnO_2 nanowires and nanorods. *Journal of Solid State Chemistry*, *179*(6), 1757-1761.
29. Chabre, Y., & Pannetier, J. (1995). Structural and electrochemical properties of the proton/γ-MnO2 system. *Progress in Solid State Chemistry*, *23*(1), 1-130.
30. Hill, L. I., Verbaere, A., & Guyomard, D. (2002). Synthesis of alpha-, beta-, and low defect gamma-manganese dioxides using the electrochemical-hydrothermal method and study of their Li insertion behavior. *Journal of New Materials for Electrochemical Systems*, *5*(2), 129-134.
31. Liu, C., Wang, J., Tian, J., & Xiang, L. (2013). Synthesis and surface characterization of γ-MnO_2 nanostructures. *Journal of Nanomaterials*, *2013*, 31.
32. Benhaddad, L., Makhloufi, L., Messaoudi, B., Rahmouni, K., & Takenouti, H. (2011). Reactivity of nanostructured MnO_2 in alkaline medium studied with a microcavity electrode: effect of oxidizing agent. *Journal of Materials Science & Technology*, *27*(7), 585-593.
33. Julien, C. M., Massot, M., & Poinsignon, C. (2004). Lattice vibrations of manganese oxides: Part I. Periodic structures. *Spectrochimica Acta Part A: Molecular and Biomolecular Spectroscopy*, *60*(3), 689-700.
34. Fernandes, J. B., Desai, B., & Dalal, V. K. (1983). Studies on chemically precipitated Mn (IV) oxides—I. *Electrochimica Acta*, *28*(3), 309-315.
35. Ananth, M. V., Pethkar, S., & Dakshinamurthi, K. (1998). Distortion of MnO_6 octahedra and electrochemical activity of Nstutite-based MnO_2 polymorphs for alkaline electrolytes—an FTIR study. *Journal of Power Sources*, *75*(2), 278-282.